ANALYSIS OF IMAGING ALGORITHMS

FOR SHAPE DETECTION*

3.1   Introduction

For highly accurate information about the target location and its shape, a high-resolution image of the target is required. Thus, one of the significant challenges in TWI is to develop an efficient imaging algorithm that can give maximum information about target [Baranoski (2008)]. In the previous articles, various imaging algorithms reported in the literature. The most commonly used algorithm for image formations is back projection, delay and sum beamforming, and frequency-wavenumber. So far, very less work has been reported in previous articles about the application of these three imaging techniques on TWI data and checking the consequences and effect of imaging. So, it becomes essential to explore the application of these algorithms on TWI data to analyze the effect of imaging and evaluating the performance. Therefore, the focus of this chapter is to apply these imaging techniques on various real TWI data and compare their results to select the effective imaging algorithm for shape detection of the target.

3.2   Imaging Algorithms

Figure 3.1 exhibit a typical geometry of through wall imaging set-up for the measurement of C-scan data. The imaging set up is placed at a fixed standoff distance, which consists of 21X 21 scan points in the XY plane. The scan point represents the position of the antenna of the SFCW radar in the XY plane when z = 0 of the 2D field scanner. The region to be imaged is located beyond the wall along the positive z-axis. At each scan point, SFCW radar transmits and receives the signal scattered from the target through the antenna. The SFCW radar transmits a wideband signal in step frequency mode in which radar sweeps through the allocated signal bandwidth via a series of narrowband signals of uniformly spaced center frequencies. The SFCW radar measures and records the

magnitude and phase of the received signal scattered from the target for various frequencies
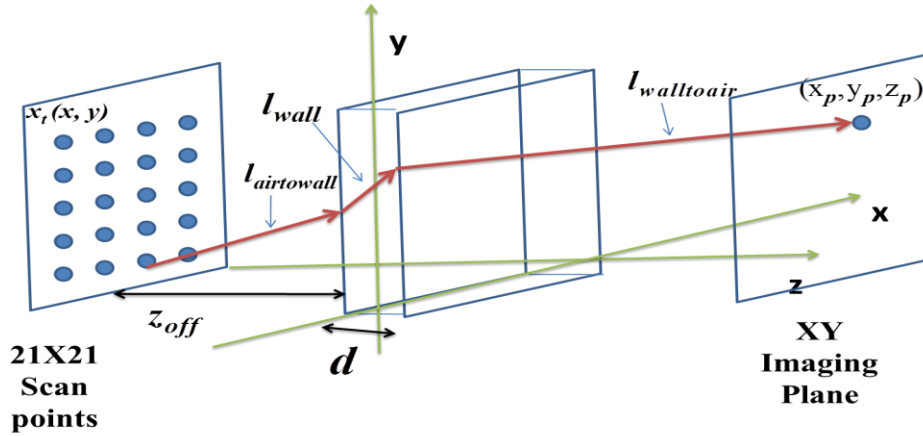
at each spatial point.

Figure 3.1. Geometric of the through wall imaging set-up [Ahmad *et al*. (2008)].

This C-scan data representing the magnitude and phase of the scattered field for various

frequencies at different scan points using SFCW radar is processed to produce a focused

image of the scene behind the wall using frequency-wave number [Hantscher *et al.* (2006)],

back-projection [Hunt (2009)], and delay and sum beamforming imaging algorithm

[Ahmad *et al.* (2008)]. Image reconstruction can be accomplished using either frequency-

domain techniques such as the Delay and Sum methods or time-domain techniques such as

backprojection [Hunt (2009), Yigit *et al.* (2007), Ozdermir *et al.* (2008)]. In backprojection

imaging technique, the received frequency domain data at each scan point are inverse

Fourier transformed to produce a range profile. For each pixel in the desired image map,

the propagation range from the scan point to the pixel and then back to the same scan point

is calculated and used to index into the range profile to find the value of the in-phase and

quadrature components of the scattered field from that range. The values of the scattered

fields obtained from all scan points are summed for each pixel in the image map. The steps

for implementation of Backprojection, and Delay and Sum Beamforming imaging

algorithm have been discussed in subsection 3.2.1 and 3.2.3 of this Chapter 3. The delay and sum imaging algorithm derived from the beamforming algorithm is a traditional frequency-domain algorithm and is also widely used for focusing in TWI systems [Ahmad *et al.* (2008)]. For cases where the frequency steps are not even, images are formed by delay and sum imaging algorithm [Hunt (2009)]. In this method, for each pixel in the image, the frequency data are phase adjusted one frequency at a time. The frequency-wavenumber imaging algorithm is also a traditional frequency-domain algorithm used for focusing in TWI and GPR [Hantscher *et al.* (2006), Yigit *et al.* (2007), Ozdemir *et al.* (2008)]. This algorithm has lower computation time compared to the back-projection and delay and sum imaging algorithms. Brief discussions about the implementation of these imaging algorithms on C-scan data to produce a focused image of the target are as follows.

3.2.1   *Backprojection*

Let the region to be imaged located beyond the wall along the positive *z*-axis is divided into pixels in downrange, crossrange, and height, represented by the *z*, *x*, and *y* coordinates, respectively. The magnitude and phase of the scattered field from P point target located at position x_{p_i}, y_{p_i}, z_{p_i} behind wall for various frequencies at different scan points position x_t, y_t using SFCW radar can be given as [Hunt (2009)]

$$S_{11}(x_t, y_t, f) = \sum_{i=1}^{P} a\left(x_{p_i}, y_{p_i}, z_{p_i}\right) \exp\left(-\alpha\left(j2\pi f \tau_{p_i}\right)\right) \qquad (3.1)$$

where f_k is frequency point, τ_{p_i} is the propagation delay from the scan point at position x, y to the pixel at position $x_{p_i}, y_{p_i}, z_{p_i}$ and then back to the same scan point, $a\left(x_{p_i}, y_{p_i}, z_{p_i}\right)$ is target reflectivity and α is attenuation constant of wall. The received data at each scan

point is Inverse Fourier transformed to produce a range profile using equation (3.2) as proposed in reference [Verma *et al.* (2009)].

$$S(x, y, z) = \sum_{k=1}^{L} S_{11}(x, y, f_k) \exp\left(j2\pi f_k (2z/c)\right) \tag{3.2}$$

where L is number of frequency points. The value of a pixel $I\left(x_{p_1}, y_{p_1}, z_{p_1}\right)$ at position $x_{p_1}, y_{p_1}, z_{p_1}$ corresponding to a point scatter p_1 at position $x_{p_1}, y_{p_1}, z_{p_1}$ is calculated using equation (3.3) as proposed by reference [Hunt (2009)]

$$I\left(x_{p_1}, y_{p_1}, z_{p_1}\right) = \sum_{x=1}^{M} \sum_{y=1}^{N} S\left(x, y, z = R_{p_1}\right) \tag{3.3}$$

where R_{p_i} is the distance traveled from the one scan point at position x_t, y_t, $z = 0$ to the pixel at position $x_{p_1}, y_{p_1}, z_{p_1}$ and then back to the same scan point. The propagation range is used to select the range cell in the range profile to get the value of the in-phase and quadrature components of the scattered field for that range cell. The values of the in-phase and quadrature components for all the scan points are summed-up for each pixel in the image map. The traveling distances inside and outside the wall, and, subsequently can be precisely computed, given the exact knowledge of the wall thickness and its dielectric constant. The expression of R_{p_1} is given by using equation (3.4) as proposed in reference [Ahmad *et al.* (2006)]

$$R_{p_1} = 2l_{airtowall} + 2\sqrt{\varepsilon}l_{wall} + 2l_{walltoair} \tag{3.4}$$

Here, the variables $l_{airtowall}, l_{wall}, l_{walltoair}$ represent the distance travelled by a signal before, through and beyond the wall from scan point at position x_t, y_t, $z = 0$ to the target at position $x_{p_1}, y_{p_1}, z_{p_1}$.

If both image pixel at position x_{p1}, y_{p1}, z_{p1} and scan point at position x_t, $y_t, z = 0$ are at the

same height, then the problem reduces to the equivalent 2-D problem, as shown in Figure

3.2 and the expression of $l_{airtowall}, l_{wall}, l_{walltoair}$ is given by equations (3.5) to (3.7)

[Ahmad *et al.* (2008)]

$$l_{\text{walltoair}} = \frac{z_{p1} - d}{\cos \theta_{p1}} \quad , \tag{3.5}$$

$$l_{\text{airtowall}} = \frac{z_{\text{off}}}{\cos \theta_{p1}} \quad , \tag{3.6}$$

$$l_{\text{wall}} = \frac{d}{\cos \psi_{p1}} \tag{3.7}$$
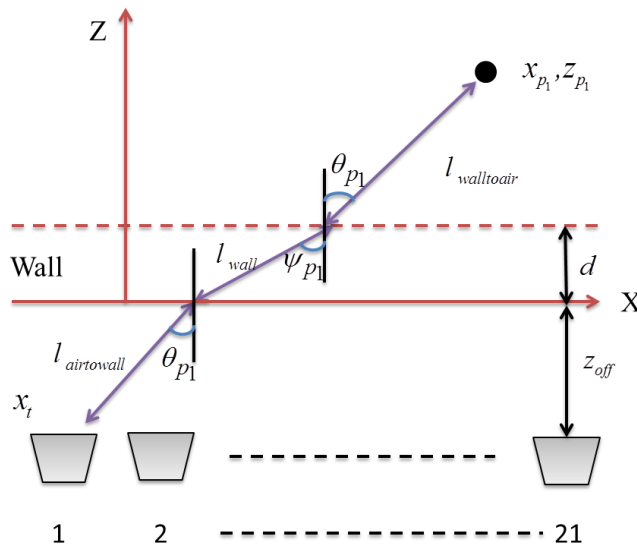
Figure 3.2. Geometry of equivalent 2-D problem when the antenna position and the image pixel are at the same height [Ahmad *et al.* (2008)].

If image pixel and antenna are at different height then a rotation transform has been applied

to x, y, z coordinate system such that angle of incidence is preserved so that in new

coordinate system image pixel and antenna appears to be at the same height. This

transformation is given by[Ahmad *et al.* (2008)]

$$\begin{bmatrix} x_t' \\ y_t' \end{bmatrix} = \begin{bmatrix} \cos\beta & \sin\beta \\ -\sin\beta & \cos\beta \end{bmatrix} \begin{bmatrix} x_t \\ y_t \end{bmatrix} \tag{3.8}$$

$$\begin{bmatrix} x_{p1}' \\ y_{p1}' \end{bmatrix} = \begin{bmatrix} \cos\beta & \sin\beta \\ -\sin\beta & \cos\beta \end{bmatrix} \begin{bmatrix} x_{p1} \\ y_{p1} \end{bmatrix} \tag{3.9}$$

$$\tan\beta = \frac{y_t - y_{p1}}{x_t - x_{p1}} \tag{3.10}$$

$$y_t' = y_{p1}' \tag{3.11}$$

Here x_t and y_t are antenna position in 2D field scanner, and x_{p1} and y_{p1} are pixel position in imaging plane. Similarly for P point scatterer at positions x_{pi}, y_{pi}, z_{pi}, the value of pixel at different P positions x_{pi}, y_{pi}, z_{pi} is given using equation (3.12) [Ahmad *et al.* (2008)]:

$$I\left(x_{pi}, y_{pi}, z_{pi}\right) = \sum_{x=1}^{M} \sum_{y=1}^{N} S\left(x, y, z = R_{pi}\right) \tag{3.12}$$

The above backprojection imaging algorithm can be implemented in the following steps as shown in Figure 3.3 and summarized as follows:

i.   The C-scan data representing back-scattered electric field $S_{11}\left(x_t, y_t, f_k\right)$ in the frequency domain is collected.

ii. The data received at each scan point is Inverse Fourier Transformed to produce a range profile.

iii. The whole image map is divided into small pixels.

iv. The propagation range is calculated from one of scan point to the pixel position and then back to the same scan point for each pixel in the desired image-map

v.   The propagation range calculated is further used to select the range bin in the range profile

vi. The Corresponding received range bin amplitude value of the scattered field is recorded.

vii. The above step is repeated for all scan points.

viii. The value of the recorded amplitude value from all scan points are added for each pixel in the image map.

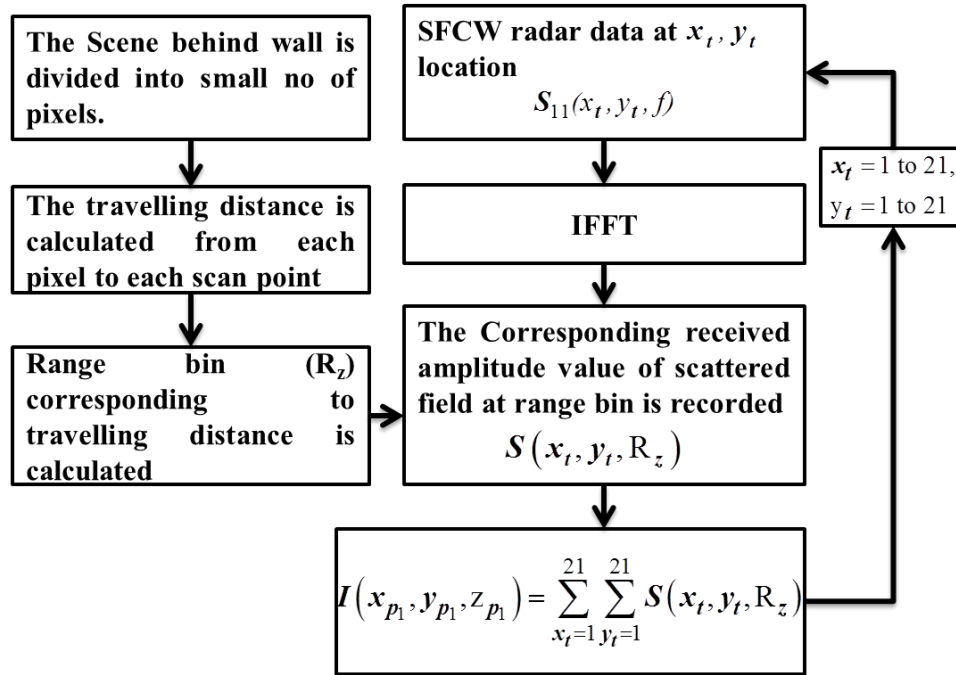

Figure 3.3. Flowchart for the implementation of backprojection imaging algorithm.

3.2.2   Delay and Sum Beamforming

Let the region to be imaged located beyond the wall along the positive z-axis is divided into pixels in downrange, crossrange, and height, represented by the z, x, and y coordinates, respectively. The magnitude and phase of the scattered field from a point target located at position x_{p1}, y_{p1}, z_{p1} beyond for various frequencies at different scan points using SFCW radar can be given as [Hunt (2009)]:

$$S_{11}(x_t, y_t, f) = a\left(x_{p1}, y_{p1}, z_{p1}\right) \exp\left(-\alpha\left(j2\pi f \tau_{p1}\right)\right) \tag{3.13}$$

For calculating the value of a pixel at position x_{p1}, y_{p1}, z_{p1} in the desired image, the propagation delay from the one scan point to the pixel and then back to the same scan point is calculated using equation (3.14) as proposed by Ahmad *et al.* (2008):

$$\tau_p = \frac{2l_{airtowall}}{c} + \frac{2l_{wall}}{v} + \frac{2l_{walltoair}}{c} \tag{3.14}$$

Here c is the velocity of signal propagation in air, and v is the velocity of signal propagation through the wall. The variable $l_{airtowall}$, l_{wall}, and $l_{walltoair}$ represent the distance travelled by a signal before, through, and beyond the wall from scan point at position x_t, y_t to the target at position $x_{p_1}, y_{p_1}, z_{p_1}$. The expression of $l_{airtowall}, l_{wall}, l_{walltoair}$ is given in previous section.

After applying delays to the outputs of the C-scan data to synchronize the signal arrived all scan points and then summing the delayed signals, the value of a pixel at position $x_{p_1}, y_{p_1}, z_{p_1}$ is estimated using equation (3.15) [Ahmad $et\ al.$ (2008)]

$$I(x_{p_1}, y_{p_1}, z_{p_1}) = \sum_{x_t=1}^{M} \sum_{y_t=1}^{N} \sum_{k=1}^{201} S_{11}(x_t, y_t, f_k) exp\left(j\,2\pi f_k \tau_{p_1}\right) \tag{3.15}$$

Similarly for P point scatterer at positions $x_{p_i}, y_{p_i}, z_{p_i}$, the value of each pixel at different P positions $x_{p_i}, y_{p_i}, z_{p_i}$ is given by equation (3.16) [Ahmad $et\ al.$ (2008)]:

$$I(x_{p_i}, y_{p_i}, z_{p_i}) = \sum_{x_t=1}^{21} \sum_{y_t=1}^{21} \sum_{k=1}^{201} \sum_{i=1}^{P} S11(x_t, y_t, f_m) exp\left(j\,2\pi f_k \tau_{p_i}\right) \tag{3.16}$$

The above delay and sum beamforming imaging algorithm can be implemented in the following steps as shown in Figure 3.4 and summarized as follows:

i.   The C-scan data representing back-scattered electric field $S_{11}(x_t, y_t, f_k)$ in the frequency domain collected. Divide the whole image map into small pixels.

ii. The propagation delay is calculated from one of scan point to the pixel position and then back to the same scan point for each pixel in the desired image-map

iii. The propagation delay applied to the data collected at each antenna location for all frequency points.

iv. The received data for all the frequency points added.

v. The above step repeated for all scan points.

vi. The result obtained for all scan points is summed to form the image.
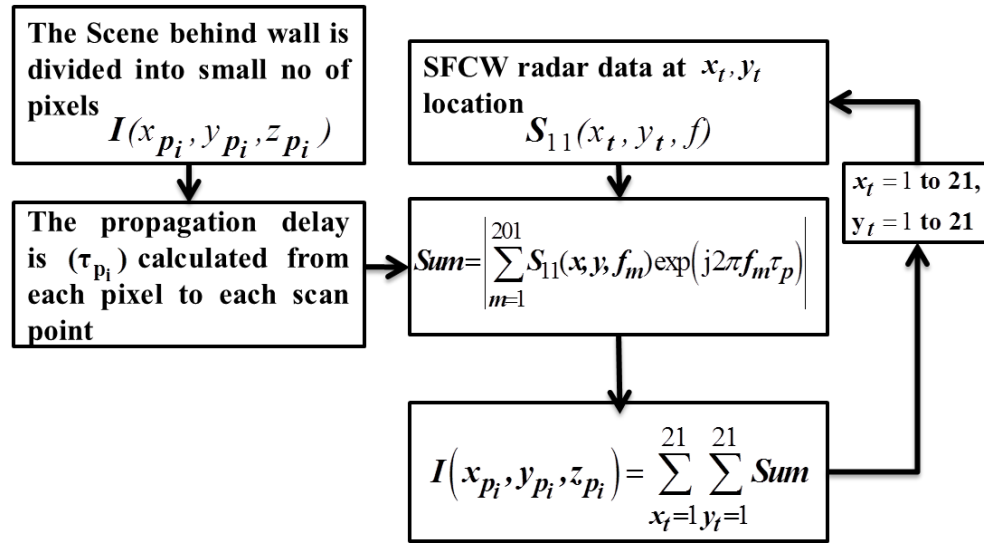
Figure 3.4. Flowchart for the implementation of delay and sum beamforming imaging algorithm.

3.2.3 *Frequency-wavenumber*

For the SFCW system, the received signal measured at scan point scattered from point target in terms of wavenumber given as [Yigit *et al.* (2007), Ozdemir *et al.* (2008)]

$$S_{11} (x_t, y_t, f) = \rho.\exp(-j2kd) \tag{3.17}$$

Where $k = 2\pi f/v$ is the wavenumber vector and ρ is the strength of the field scattered from the point target The received field from *P* point targets located at different positions $x_{p_i}, y_{p_i}, z_{p_i}$ assuming homogeneous wall is given as [Yigit *et al.* (2007), Ozdemir *et al.* (2008)]

$$S_{11}(x_t,y_t,f) = \sum_{i=1}^{P}\rho_i.\exp\left(-jk\left(2\sqrt{z_{p_i}^2 + (x_t - x_{p_i})^2 + (y_t - y_{p_i})^2}\right)\right) \tag{3.18}$$

Applying two-dimensional 2D Fourier transform to S_{11} (x_t, y_t, f) along the x-direction and

y-direction, the frequency-wavenumber domain representation of scattered data given as

[Hantscher *et al.* (2006)]:

$$S(k_x,k_y,f) = \sum_{i=1}^{P}\rho_i.\int_{\infty}^{\infty}\int_{-\infty}^{\infty}\exp\left(-jk\left(2\sqrt{z_i^2 + (x - x_i)^2 + (y - y_i)^2}\right)\right).\exp\left(jk_x x\right)dx\exp\left(jk_y y\right)dy$$

$$\tag{3.19}$$

This is the received signal data in $k_x k_y$–f domain. It can be assumed that a total of P point

targets ideally imaged in real coordinates as

$$S(x,y,z) = \sum_{i=1}^{P}\rho_i.\,\delta(x - x_{p_i}, y - y_{p_i}, z - z_{p_i}) \tag{3.20}$$

Where $\delta(x, y, z)$ is the two-dimensional impulse function. After, applying the three

dimensional Fourier transform to this ideal image data with respect to $x, y,$ and $z,$ the

following scattered field value $\bar{S}(k_x,k_y,k_z)$ in the spatial-frequency domain is obtained

which is given as

$$\bar{S}(k_x,k_y,k_z) = \sum_{i=1}^{P}\rho_i.\exp\left(-jk_x x_{p_i} - jk_y y_{p_i} - jk_z z_{p_i}\right) \tag{3.21}$$

Then, the mapping of $S(k_x,k_y,f)$ data is done from $k_x k_y$ domain to the $k_x k_y k_z$ domain by

using interpolation to obtain $\bar{S}(k_x,k_y,k_z)$ by relating the values of $S(k_x,k_y,f)$ at each f

point to the values of $\bar{S}(k_x,k_y,k_z)$ at k_z points with the help of the frequency mapping

equation $k_z = \sqrt{4k^2 - k_x^2 - k_y^2}$ Afterward, the final focused image spotting the true locations

of the target obtained by taking the two-dimensional IFFT of $\overline{S}$ (k_x,k_y,k_z) is given as

[Hantscher *et al.* (2006), Yigit *et al.* (2007)]

$$I(x_{p_i}, y_{p_i}, z_{p_i}) = \frac{1}{(2\pi)^3} \int\limits_{-\infty}^{\infty} \int\limits_{-\infty}^{\infty} \int\limits_{-\infty}^{\infty} \overline{S}(k_x,k_y,k_z) \; \exp\left(jk_x x + jk_y y + jk_z z \right) dk_x dk_y dk_z$$

(3.22)

Here, $I(x_{p_i}, y_{p_i}, z_{p_i})$ representing the value of a pixel at the position $x_{p_i}, y_{p_i}, z_{p_i}$ in the image domain.

The above frequency-wavenumber imaging algorithm can be implemented in the following steps as shown in Figure 3.5 and are listed below:

   i. The C-scan data representing back-scattered electric field $S_{11}(x_t, y_t, f_k)$ in the frequency domain collected.

   ii. A two dimensional Fourier transform is applied on $S_{11}(x_t, y_t, f)$ along synthetic aperture *x and y* to get $S(k_x, k_y, f)$ and normalized it.

   iii. $S(x, y, f)$ is interpolated to $k_x k_y k_z$ domain to obtain $\overline{S}(k_x, k_y, k_z)$

   iv. A three-dimensional IFFT $\overline{S}(k_x, k_y, k_z)$ is taken to form the final focused three-dimension image $I(x_{p_i}, y_{p_i}, z_{p_i})$ in Cartesian coordinates.

<div style="border:1px solid black; text-align:center;">

SFCW radar data at x_t, y_t location

$$S_{11}(x_t, y_t, f)$$

</div>

$\downarrow$

<div style="border:1px solid black; text-align:center;">

Take 2D FFT to get $S(k_x, k_y, f)$

</div>

$\downarrow$

<div style="border:1px solid black; text-align:center;">

$S(x, y, f)$ is interpolated on to $k_x k_y k_z$ domain to obtain $S(k_x, k_y, k_z)$

</div>

$\downarrow$

<div style="border:1px solid black; text-align:center;">

Take 3D IFFT to obtain

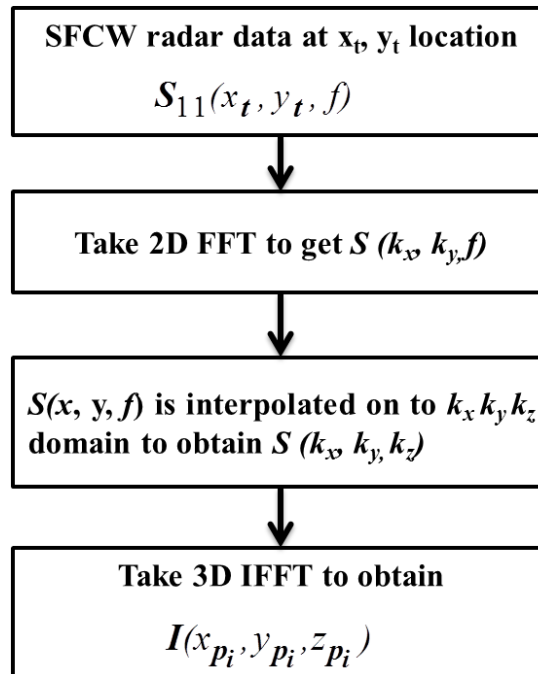$$I(x_{p_i}, y_{p_i}, z_{p_i})$$

</div>

Figure 3.5. Flowchart for the implementation of frequency-wavenumber imaging algorithm.

3.3.   Results and Discussion

To analyze the effect of imaging algorithms on real data an experiment is carried-out with the help of a monostatic SFCW radar system. The acquired C-scan data is processed further for the formation of 2D C-scan through-the-wall radar images using back projection, frequency-wavenumber, and delay and sum beamforming. Before forming the 2D C-scan through-the-wall radar image of the target, it is essential to know the characteristics of the wall, presence of the target and its location. These things affect the quality of the image. Estimation of wall dielectric has been done in a similar manner as proposed by Muqaibal and Safaai-Jazi (2003), as discussed in Chapter 2. The dielectric value of the wall has found to be 6.4.For finding target location, the range profile at one of

the scan point from the measured C-scan data using measurement set-up is analyzed. The range profile can be represented as [Chandra *et al.* (2011)]:

$$S(z) = \sum_{k=1}^{201} S(f_k) \exp\left(j2\pi f_k (2z/c + t_{delay} + 2d(\sqrt{\varepsilon'} - 1)/c)\right) \tag{3.23}$$

where t_{delay} is delay due to antenna system, d is wall thickness, ε' is wall dielectric, and f_k is frequency. To estimate the delay due to the antenna system, a separate experiment is carried out similar to as described in Chapter 2. Figure 3.6 shows the range profile plot for one of the scan point of the C-scan data at which target reflections occurs.
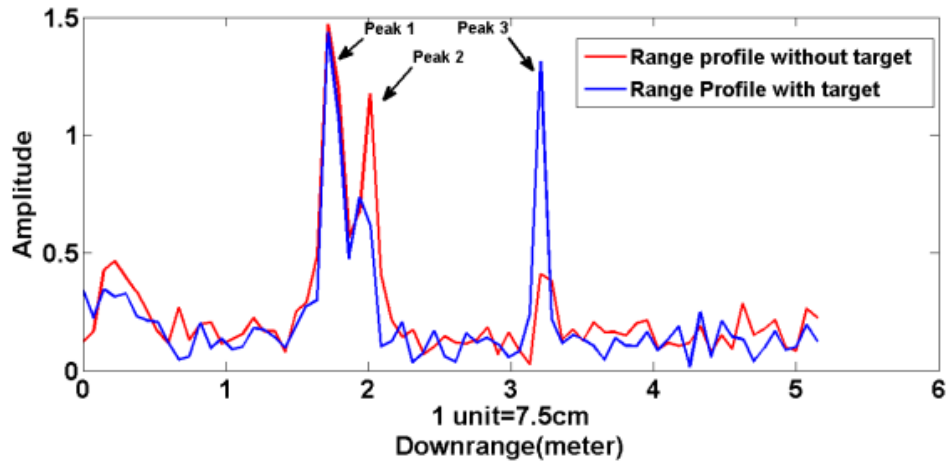

Figure 3.6. Range profile plot

In the range profile plot shown, the first two peaks are due to reflection from the front and rear side of the wall, and the third peak show reflection from the target. The target downrange location is calculated from the range profile. Once target downrange position is estimated, the two-dimensional image of the target (horizontal cross-range vs vertical cross-range) using backprojection, frequency-wavenumber, and delay and sum beamforming algorithms is plotted by considering a Y plane at a fixed target range bin ($z = z_{target}$), which got selected by observing the range profile. Thus, a virtual imaging plane of size 50X50 pixels is formed.

Different imaging algorithms are applied on acquired C-Scan data with various shapes of considered targets S1, S2, S3, and S4 to analyze the effect the imaging. The details of target is given in Table 3.1

Table 3.1 Details of target samples considered

Target ID	Shape	Size (Length X Width)	Orientation	Material
S1	Circle	Dia=30cm	0	Metal
S2	Circle	Dia=35cm	0	Metal
S3	Square	30cmX30cm	0	Metal
S4	Rectangle	50cmX30cm	0	Metal

The 2D through-the-wall radar image of considered targets using each imaging algorithm is shown in Figures 3.7 (a-l). In Figures 3.7 (a-l), X-axis represents cross-range and Y-axis represents the height of the target. The Shape of the target is extracted after thresholding the 2D C-scan through-the-wall radar image using statistical method. The threshold value is obtained using equation (3.23) which is given by

$$Th = \mu + \sigma \tag{3.24}$$

where μ is mean and σ is standard deviation. The thresholded 2D C-scan through-the-wall radar image shape of considered targets using each imaging algorithm is shown in Figures 3.8 (a-p) along with the reference shape of the target. The number of target pixels of reference target shape is obtained based on a priori information of target size, location, and size of pixel [Tiwari *et al.* (2009), Ibrahim *et al.* (2014), Kumar *et al.* (2017)]. As per experimental results with various target samples, a considerable difference between the output images of algorithms from the focusing point of view is observed.
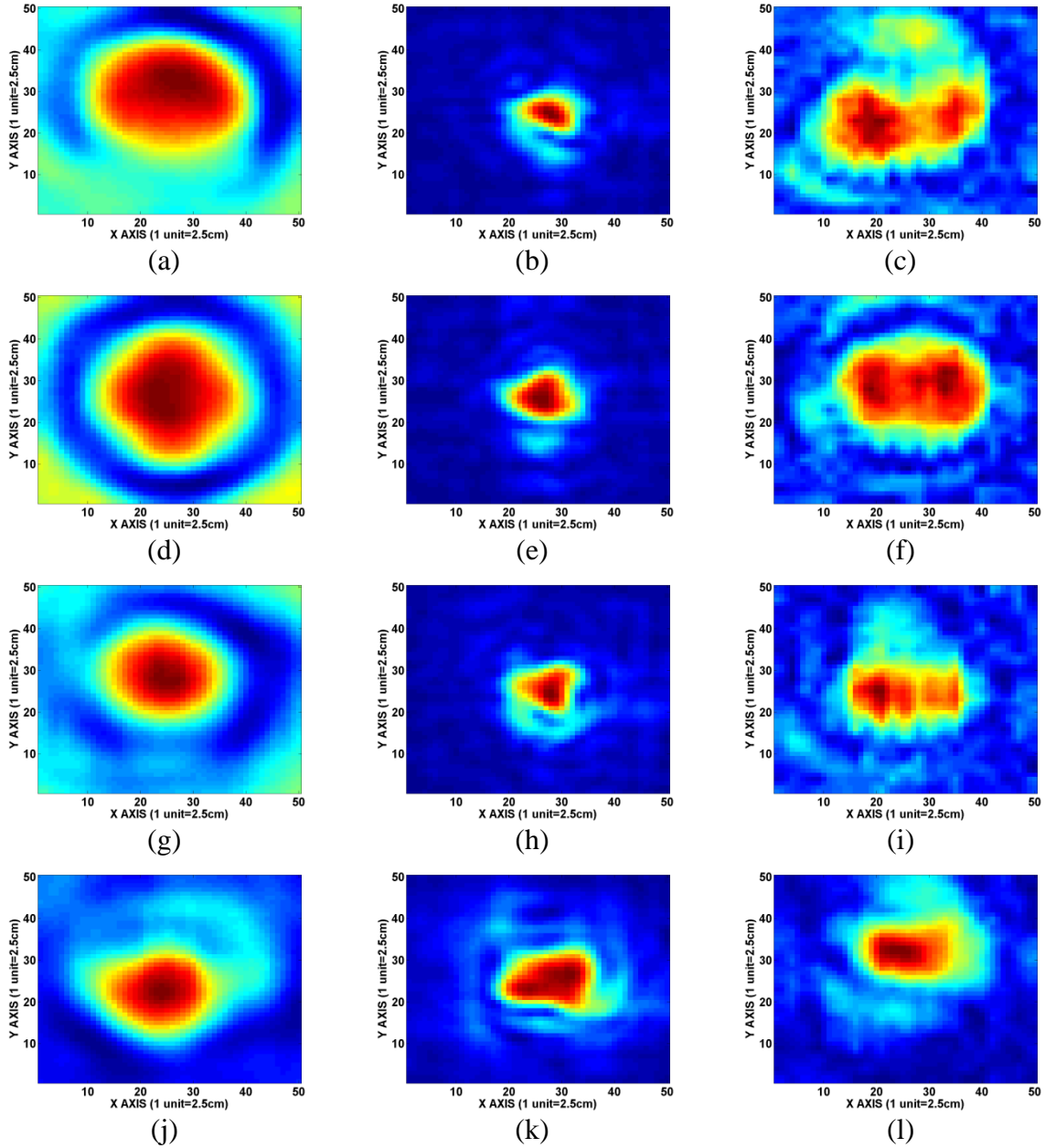
(a)   (b)   (c)

(d)   (e)   (f)

(g)   (h)   (i)

(j)   (k)   (l)

Figure 3.7.(a) 2D C-Scan through-the-wall radar image obtained using backprojection imaging method on imaging plane along X and Y axis of target id S1.**(b)** 2D C-Scan through-the-wall radar image obtained using delay and sum beamforming imaging method on imaging plane along X and Y axis of target id S1.**(c)** 2D C-Scan through-the-wall radar image obtained using frequency-wave number imaging method on imaging plane along X and Y axis of target id S1.**(d)** 2D C-Scan through-the-wall radar image obtained using backprojection imaging method on imaging plane along X and Y axis of target id S2.**(e)** 2D C-Scan through-the-wall radar image obtained using delay and sum beamforming imaging method on imaging plane along X and Y axis of target id S2.**(f)** 2D C-Scan through-the-wall radar image obtained using frequency-wavenumber imaging number

method on imaging plane along X and Y axis of target id S2.**(g)** 2D C-Scan through-the-wall radar image obtained using backprojection imaging method on imaging plane along X and Y axis of target id S3.**(h)** 2D C-Scan through-the-wall radar image obtained using delay and sum beamforming imaging method on imaging plane along X and Y axis of target id S3.**(i)** 2D C-Scan through-the-wall radar image obtained using frequency-wavenumber imaging method on imaging plane along X and Y axis of target id S3.**(j)** 2D C-Scan through-the-wall radar image obtained using back projection imaging method on imaging plane along X and Y axis of target id S4.**(k)** 2D C-Scan through-the-wall radar image obtained using delay and sum beamforming imaging method on imaging plane along X and Y axis of target id S4.**(l)** 2D C-Scan through-the-wall radar image obtained using frequency-wavenumber imaging method on imaging plane along X and Y axis of target id S4.
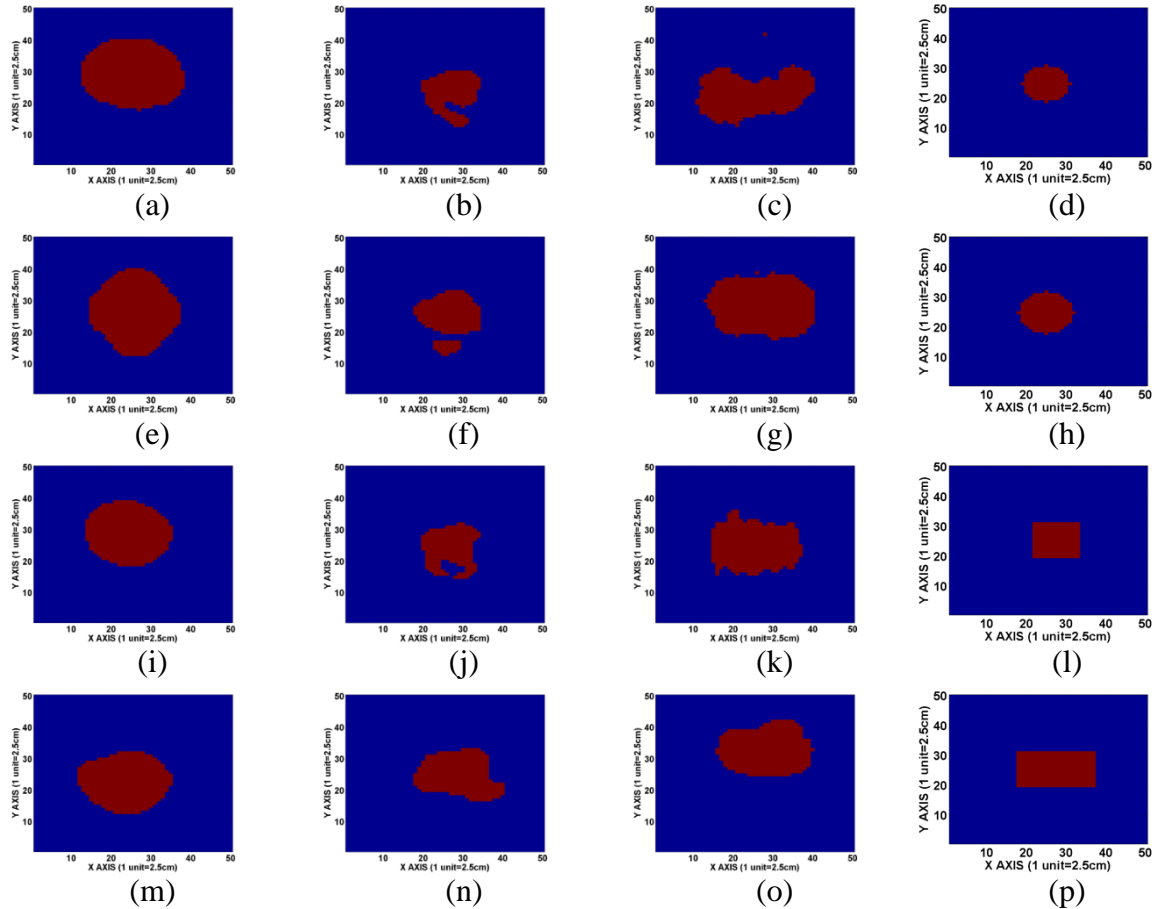

Figure 3.8.(a) Thresholded 2D C-Scan through-the-wall radar image obtained using backprojection imaging method on imaging plane along X and Y axis of target id S1.**(b)** Thresholded 2D C-Scan through-the-wall radar image obtained using delay and sum imaging method on imaging plane along X and Y axis of target id S1.**(c)** Thresholded 2D C-Scan through-the-wall radar image obtained using frequency wave number imaging method on imaging plane along X and Y axis of target id S1.**(d)**Reference target shape of

target id S1.**(e)** Thresholded 2D C-Scan through-the-wall radar image obtained using back projection imaging method on imaging plane along X and Y axis of target id S2.**(f)** Thresholded 2D C-Scan through-the-wall radar image obtained using delay and sum imaging method on imaging plane along X and Y axis of target id S2.**(g)** Thresholded 2D C-Scan through-the-wall radar image obtained using frequency wave number imaging method on imaging plane along X and Y axis of target id S2,**(h)** Reference target shape of target id S2.**(i)** Thresholded 2D C-Scan through-the-wall radar image obtained using back projection imaging method on imaging plane along X and Y axis of target id S3.**(j)** Thresholded 2D C-Scan through-the-wall radar image obtained using delay and sum imaging method on imaging plane along X and Y axis of target id S3.**(k)** Thresholded 2D C-Scan through-the-wall radar image obtained using frequency wave number imaging method on imaging plane along X and Y axis of target id S3, **(l)**Reference target shape of target id S3.**(m)** Thresholded 2D C-Scan through-the-wall radar image obtained using back projection imaging method on imaging plane along X and Y axis of target id S4.**(n)** Thresholded 2D C-Scan through-the-wall radar image obtained using delay and sum imaging method on imaging plane along X and Y axis of target id S4.**(o)** Thresholded 2D C-Scan through-the-wall radar image obtained using frequency wave number imaging method on imaging plane along X and Y axis of target id S4.**(p)**Reference target shape of target id S4.

From Figures 3.8(a-p), it can be observed that though the considered imaging algorithm has accurately detected the position of the target, backprojection and frequency-wavenumber imaging algorithm perform poorly in detecting approximate sizes and shapes of the target. The shape and size of the target detected are also compared with the reference target shape. The comparison between the number of target pixels detected using each imaging algorithm and the number of target pixels in reference target shape is shown in Table 3.2. From Table 3.2, it can easily be observed that with the delay sum imaging technique, the numbers of target pixels detected are close to the number of target pixels of reference target shape as compare to frequency-wavenumber and backprojection imaging technique. This shows that delay and sum imaging algorithm prove to be a more effective imaging tool compared to backprojection and frequency-wavenumber imaging algorithms for detecting approximate shape and size of the target.

Table 3.2. No. of target pixels in thresholded 2D C-Scan through-the-wall radar image of the considered target using different imaging algorithm.

Targets	No. of targets pixels detected In Backprojection image	No. of target pixels detected In Delay and Sum beamformed image	No. of target pixels detected In Frequency-Wavenumber image	No. of target pixels in Reference target shape
S1	470	173	381	144
S2	470	210	466	196
S3	362	184	351	144
S4	362	272	342	240

Moreover, we have analyzed the useful information about the statistics of the target image formed with considered imaging algorithms. Using the thresholded binary image, the 2D C-Scan through-the-wall radar image is masked, producing 2D C-Scan through-the-wall radar image with the target region only. The statistics of the target image have been obtained using commercially available easyfit software [Easyfit]. Various probability density functions, which were available in easyfit software, are analyzed for evaluating the probability density function of the target image. For evaluating the probability density function target image, a Kolmogorov-Smirnov (KS) goodness of fit test is performed on various probability density functions. Only those pdf functions are selected, which have passed the KS test on the basis that statistic value should be less than critical value and that p-value is greater than the level of significance (5%). The probability density functions of the target image are evaluated for considered targets of different shapes for each imaging algorithm. The pdf of the target image of the considered target for each imaging algorithm is shown in Table 3.3. From Table 3.3, it is observed that the probability distribution of the target images changes with imaging algorithm. For example, back-projection and beamforming have Beta distribution, whereas frequency-wavenumber has Weibull

distribution. The probability density function of Weibull and Beta is given by [Forbes*et al.* (2011)]

$$f(x) = \frac{\chi_1}{\chi_2}\left(\frac{x-y}{\chi_2}\right)^{\chi_1-1} \exp\left(\frac{x-\chi_3}{\chi_2}\right)^{\chi_1} \tag{3.25}$$

where χ_1, χ_2 are shape parameter, and χ_3 continuous location parameter.

$$f(x) = \frac{1}{B(\zeta_1,\zeta_2)} \frac{(x-g)^{\zeta_1-1}(b-x)^{\zeta_2-1}}{(b-g)^{\zeta_1+\zeta_2-1}} \tag{3.26}$$

where ζ_1 and ζ_2 are shape parameter, b and g are continuous boundary parameter.

Table 3.3. KS statistics and fitting parameter for distributions of target image in 2D C-Scan through-the-wall radar image for targets S1, S2, S3, and S4 for different imaging algorithm.

Imaging Algorithms	Pdf	Statistics	Target S1	Target S2	Target S3	Target S4
Backprojection	Beta	Statistics	0.02683	0.0176	0.01701	0.01944
		P-value	0.87848	0.99815	0.9999	0.99881
		Critical value	0.06264	0.06264	0.07137	0.07137
		Fitting Parameters	ζ_1=1.1474 ζ_2=1.0165 g=0.68875 b=1.0	ζ_1=0.96525 ζ_2=0.81424 g=0.68231 b=1.0	ζ_1=0.94697 ζ_2=0.99075 g=0.54975 b=1.0	ζ_1=0.90775 ζ_2=1.0182 g=0.51176 b=1.0
Delay and Sum Beamforming	Beta	Statistics	0.07459	0.05245	0.04368	0.05667
		P-value	0.27683	0.59145	0.85869	0.33415
		Critical value	0.10325	0.09371	0.10011	0.08234
		Fitting Parameters	ζ_1=0.55899 ζ_2=1.1222 g=0.27584 b=1.0125	ζ_1=0.62207 ζ_2=0.87022 g=0.26461 b=1.0	ζ_1=0.61138 ζ_2=1.0845 g=0.3427 b=1.0	ζ_1=0.75844 ζ_2=0.739 g=0.39348 b=1.0
Frequency-wavenumber	Weibull	Statistics	0.04569	0.05318	0.06759	0.0698
		P-value	0.39223	0.13821	0.07726	0.06803
		Critical value	0.06957	0.06291	0.07248	0.07343
		Fitting Parameters	χ_1=1.6266 χ_2=0.17504 χ_3=0.60852	χ_1=3.7796 χ_2=0.38852 χ_3=0.43273	χ_1=1.9381 χ_2=0.28158 χ_3=0.41659	χ_1=1.287 χ_2=0.24285 χ_3=0.42861

It can also be observed that the pdf of the target image with delay sum imaging algorithm, back projection and frequency-wavenumber imaging technique appears to consistently follow a single probability density function for different considered targets. This shows that a single probability density based function captures the true properties of the backscattered signal. However, the shape parameter of Weibull distribution changes with the small change in target geometry and shape parameter of beta distribution remain almost constant with change in target geometry. This shows that a small change in target geometry provides a large change in the probability distribution of target image with a frequency-wavenumber algorithm, hence the possibility of the false alarms rate while performing detection of the target will be higher with frequency-wavenumber imaging algorithm and will be lower with back-projection and delay and sum beamforming imaging technique.

Further, to analyze quality of 2D C-Scan through-the-wall radar image of the target with these imaging algorithms, Peak to Signal Noise ratio (PSNR) is computed. The PSNR is computed using equations (3.27) and (3.28) which is given by:

$$MSE = \frac{1}{UXV}\sum_{i=1}^{V}\sum_{j=1}^{U}\left(F(\text{i},\text{j}) - I(\text{i},\text{j})\right)^{2} \tag{3.27}$$

$$PSNR(\text{dB}) = 10\log\left(\frac{1}{MSE}\right) \tag{3.28}$$

where *I* represent a 2D C-scan through-the-wall radar image (TWRI) without a target, *F* represent a 2D C-Scan through-the-wall radar image with the target, *U* represents no of pixels in row, and *V* represents number of pixels in the columns. Image quality of different algorithms can be visibly observed from the obtained results. From Table 3.4, it can be observed that peak to signal noise of formed images using delay and sum beamforming

imaging technique is high and closely followed by backprojection and frequency-wavenumber imaging algorithm.

Table 3.4. PSNR (dB) value of imaging algorithm for target id S1, S2, S3, S4.

Targets	Backprojection	Delay and Sum Beamforming	Frequency-wavenumber
S1	9.3175	11.7132	10.9223
S2	9.2833	11.4005	10.5186
S3	11.2491	11.8652	12.1104
S4	11.4193	11.7823	11.7669

A high PSNR shows that a good contrast is present between the pixels corresponding to the target and the background pixels. Thus, the shape of the target can be easily detected.

In the present chapter, our main aim is to select an efficient image reconstruction algorithm that can give maximum information about targets such as its location, approximate shape, and size. For this purpose, we have analyzed the effect of delay and sum beamforming, backprojection, and frequency-wavenumber imaging algorithms on approximate shape and size of the target, peak to signal noise ratio of image, and probability distribution of target image with different shape and size of TWI data. For detecting target pixels with a low false alarm, the probability distribution of target image should not change with target geometry, and the contrast of image should be high. From the experimental results, it is observed that peak to signal noise of formed images using delay and sum beamforming imaging technique is high and closely followed by backprojection and frequency-wavenumber imaging algorithm, which shows that a high-quality 2D C-Scan through-the-wall radar images of the target can be obtained with delay and sum beamforming algorithm, backprojection and frequency-wavenumber imaging algorithm. It is also observed that the probability distribution of the target images changes with the imaging algorithm. For example, backprojection and beamforming have Beta distribution, whereas frequency-wavenumber has Weibull distribution. Moreover, a small

change in target geometry provides a large change in the shape parameters of Weibull distribution is observed whereas shape parameters of Beta distribution do not change much with small change target geometry. It shows that the probability distribution of frequency-wavenumber image of target changes as target geometry changes, hence possibility of the false alarms rate will be higher with frequency-wavenumber imaging algorithm. Thus, delay and sum beamforming, and backprojection algorithm are useful for detecting the location of a target with a low false alarm. However, back-projection and frequency-wavenumber imaging algorithms have poorly reconstructed approximate shape and size of the target compared to the delay and sum beamforming imaging algorithm. It is observed that with delay and sum beamforming imaging technique, numbers of target pixels detected are close to the number of target pixels of reference target shape in comparison with frequency-wavenumber and back-projection imaging technique. Thus, delay and sum beamforming, and back-projection imaging algorithms can be used to detect the target with a low false alarm, but for detecting approximate shape and size of the target, delay and sum imaging algorithm prove to be a more effective imaging tool compared to back-projection and frequency-wavenumber imaging algorithms.

3.4   Conclusion

In this chapter, our main focus was to critically analyze backprojection, delay and sum beamforming, and frequency-wavenumber imaging algorithms on real data to select an effective imaging algorithm. These imaging algorithms have been applied to C-Scan data, and a comparison of obtained images has been carried out. As per our experimental observations with various target samples, a considerable difference between the output

images of algorithms from the focusing point of view has found. Though the considered imaging algorithm can accurately locate the position of the target, backprojection and frequency-wavenumber algorithms perform poorly in detecting target sizes and shapes compare to delay sum beamforming imaging algorithms. It has been observed that peak to signal noise ratio of images formed using the delay and sum beamforming imaging algorithm is high compare to back projection and frequency-wavenumber imaging algorithms. It has also been observed delay and sum beamforming imaging algorithm can be effectively used to detect approximate shape and size of the target with low false alarm as compare to frequency-wavenumber and back projection. However, the processing time required for the delay and sum algorithm is high as compared to the frequency-wavenumber algorithm.